J. Fluid Mech. (1991), *vol.* 231, *pp.* 545–560
Printed in Great Britain

Viscous motion of disk-shaped particles through parallel-sided channels with near-minimal widths

By D. HALPERN[1] AND T. W. SECOMB[2]

[1] Biomedical Engineering Department, Northwestern University, Evanston IL 60208, USA
[2] Department of Physiology, University of Arizona, Tucson, AZ 85724, USA

(Received 7 March 1990 and in revised form 19 November 1990)

The motion of a rigid disk-shaped particle with rounded edges, which fits closely in the space between two parallel flat plates, and which is suspended in a viscous fluid subject to an imposed pressure gradient, is analysed. This problem is relevant to the squeezing of red blood cells through narrow slot-like channels which are found in certain tissues. Mammalian red cells, although highly flexible, conserve volume and surface area as they deform. Consequently, a red cell cannot pass intact through a channel which is narrower than some minimum width. In channels that are just wide enough to permit cell passage, the cell is deformed into its 'critical' shape: a disk with rounded edges. In this paper, the fluid mechanical aspects of such motions are considered, and the particle is assumed to be rigid with the critical shape. The channel cross-section is assumed to be rectangular. The flow of the suspending fluid is described using lubrication theory. Use of lubrication theory is justified by considering the motion of a circular cylinder between parallel plates. For disk-shaped particles, approximate solutions are obtained by applying lubrication equations throughout the flow domain. In the region beyond the particle, this is equivalent to assuming a Hele-Shaw flow. More accurate solutions are obtained by including effects of boundary layers around the particle and at the sides of the channel. Pressure distributions and particle velocities are computed as functions of geometrical parameters, and it is shown that the particle may move faster or slower than the mean velocity of the surrounding fluid, depending on the channel dimensions.

1. Introduction

The aim of this paper is to develop theoretical models for the motion of rigid disk-shaped particles through uniform channels with rectangular cross-sections of width d and 'span' a, where $d/a \ll 1$. In the spleen and in the bone marrow, red blood cells encounter narrow passages which may have the approximate form of slots. The spleen serves as a filter, and it is believed that as red cells age, they lose flexibility, become stuck in the spleen and are removed from the circulatory system. Since red cells deform at constant volume and surface area, there is a minimum spacing between the two plates below which passage of intact cells is not possible. In channels that are just wide enough to permit cell passage, the cell is deformed into its 'critical' shape: a disc with rounded edges (Halpern 1989). Here, we consider the near-critical case in which the distance between the two plates is slightly larger than the width of the particle of critical shape.

Halpern & Secomb (1989) analysed the squeezing of red blood cells through cylindrical capillaries with near-minimal diameters, and showed that the behaviour

of flexible cells was closely approximated by the behaviour of rigid cells with the critical shape, for which closed-form lubrication solutions are available (Özkaya & Skalak 1983; Özkaya 1986). By analogy, we expect that the motion of rigid particles with the critical shape approximates the motion of flexible cells in parallel-sided channels of near minimal widths. Assuming rigid particles simplifies the analysis of the fluid mechanical aspects of the problem. Evidence supporting this assumption is provided by Halpern (1989). As in other analyses of red blood cell motion in narrow conduits (Secomb *et al.* 1986; Halpern & Secomb 1989), inertial effects are neglected and lubrication theory is used since the gaps between the particle and the plates are narrow.

Red blood cells deform at constant volume and almost constant surface area. These constraints limit the possible shapes of a red blood cell lying between two parallel plates. Consequently, there exists a minimum distance between the two plates through which a cell may pass without increasing its volume and surface area. The shape in this limiting case can be determined using calculus of variations (Halpern 1989), and is a disk with a rounded edge (figure 3). The profile of the edge is closely approximated by a semicircle. In this approximation, the surface area and volume are:

$$S = 2\pi(r_1^2 + \pi w r_1 + 2w^2), \quad V = \pi w(2r_1^2 + \tfrac{4}{3}w_2 + \pi w r_1),$$

where $2w$ is the width of the particle and r_1 is the radius of the disk part. For typical dimensions $V = 90\ \mu m^3$ and $S = 135\ \mu m^2$, $r_1 = 3.25\ \mu m$ and $w = 0.91\ \mu m$.

2. Formulation using lubrication theory

In our analysis of the motion of disk-shaped particles, equations of lubrication theory are applied throughout the flow domain. This approximation greatly simplifies the analysis. Before formulating the equation, we present evidence to justify the approximation. Since the rim of the disk has a semicircular cross-section, the flow near the rim is closely related to the flow around a cylinder between two parallel plates. The application of lubrication theory to this flow is considered first, and then further evidence based on other studies is presented.

2.1. *A rigid cylinder between two plates*

We consider a freely suspended, neutrally buoyant cylinder of diameter λd midway between two plates a distance d apart, moving with velocity $-u_p$ as shown in figure 1. We use coordinates (x, y, z) fixed with the particle, and non-dimensionalize: $X = x/d$, $Z = z/d$, $U = u/u_0$, $U_p = u_p/u_0$ and $P = p/(12\mu u_0/d)$, where u is the fluid velocity in the x direction, $-u_0$ is the mean fluid velocity relative to the plates, and p is the pressure. Under the assumptions of lubrication theory, $P = P(X)$ in the gaps, and the momentum equation in the X-direction is

$$\frac{d^2U}{dZ^2} = 12\frac{dP}{dX}. \tag{2.1}$$

By symmetry, only the lower gap has to be analysed. The boundary conditions are that $U = 0$ on the cylinder ($Z = H$, where $H(X)$ is the dimensionless gap width), $U = U_p$ on the plate ($Z = 0$), and $\overline{U} \to U_p - 1$ as $X \to \pm\infty$, where $\overline{U}$ is the mean fluid velocity. From (2.1),

$$U = 6\frac{dP}{dX}Z(Z-H) + U_p\left(1 - \frac{Z}{H}\right). \tag{2.2}$$

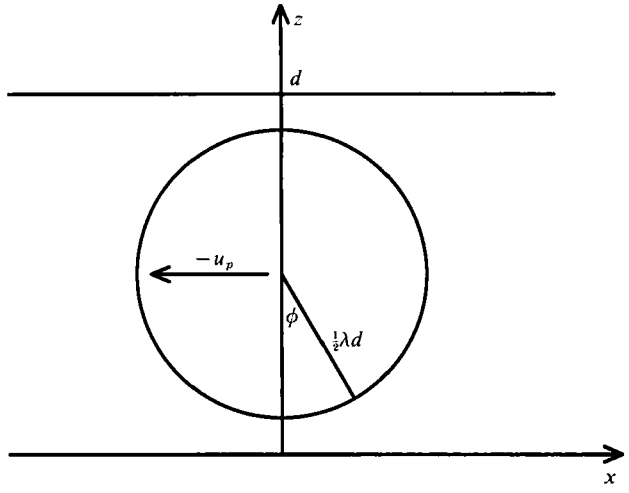

FIGURE 1. Cylinder between parallel plates, showing geometric variables.

The flow rate in the gap is

$$Q = \int_0^H U\,\mathrm{d}Z = -H^3\frac{\mathrm{d}P}{\mathrm{d}X} + \tfrac{1}{2}HU_p. \tag{2.3}$$

Hence the pressure satisfies

$$\frac{\mathrm{d}P}{\mathrm{d}X} = \tfrac{1}{2}U_p H^{-2} - QH^{-3}. \tag{2.4}$$

By continuity, $2Q$ must be constant, equal to the flow rate at infinity, $U_p - 1$.

From the assumed geometry,

$$H = \tfrac{1}{2}(1-\lambda\cos\phi), \quad X = \tfrac{1}{2}\lambda\sin\phi, \tag{2.5}$$

where ϕ is as defined in figure 1. Therefore,

$$\frac{\mathrm{d}P}{\mathrm{d}\phi} = \lambda\cos\phi\left(\frac{U_p}{(1-\lambda\cos\phi)^2} - \frac{4Q}{(1-\lambda\cos\phi)^3}\right). \tag{2.6}$$

This is integrated to yield the pressure distribution in the gap:

$$P(\phi) = \lambda(U_p I_2(\phi) - 4QI_3(\phi)), \tag{2.7}$$

where

$$I_n(\phi) = \int_0^\phi \frac{\cos t}{(1-\lambda\cos t)^n}\,\mathrm{d}t \quad (n = 1, 2, 3), \tag{2.8}$$

and, using a transformation due to Sommerfeld (1904),

$$\left.\begin{aligned} I_1(\phi) &= \frac{2\lambda^*(\phi)-\phi}{\lambda}, \quad I_2(\phi) = \frac{1}{1-\lambda^2}\left(\frac{\sin\phi}{1-\lambda\cos\phi} + 2\lambda\lambda^*(\phi)\right), \\ I_3(\phi) &= \frac{1}{2(1-\lambda^2)^2}\left(\frac{\sin\phi}{1-\lambda\cos\phi}\left(\frac{1-\lambda^2}{1-\lambda\cos\phi} + 1 + 2\lambda^2\right) + 6\lambda\lambda^*(\phi)\right), \end{aligned}\right\} \tag{2.9}$$

where

$$\lambda^*(\phi) = \frac{1}{(1-\lambda^2)^{\frac{1}{2}}}\tan^{-1}\left[\left(\frac{1+\lambda}{1-\lambda}\right)^{\frac{1}{2}}\tan\tfrac{1}{2}\phi\right]. \tag{2.10}$$

The pressure drop, ΔP, across the particle is then:

$$\Delta P = 2\lambda[(I_2(\tfrac{1}{2}\pi) - 2I_3(\tfrac{1}{2}\pi))\,U_p + 2I_3(\tfrac{1}{2}\pi)]. \tag{2.11}$$

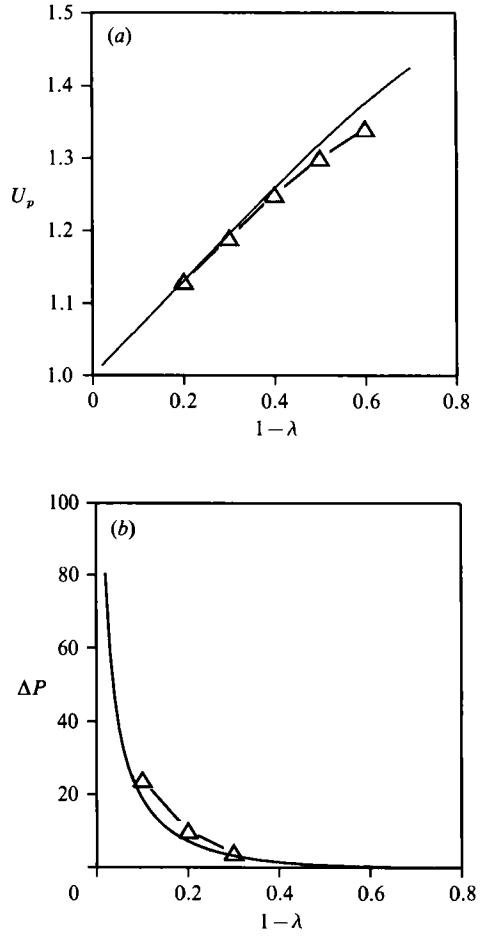

FIGURE 2. (*a*) Cylinder velocity U_p and (*b*) additional pressure drop ΔP due to cylinder, as functions of minimum gap width $(1-\lambda)$ for a cylinder in Poiseuille flow between parallel plates. ——, lubrication theory; △, finite differences method (Dvinsky & Popel 1987*b*).

The total force acting on a control volume containing the cylinder ($0 \leqslant Z \leqslant 1$, $-\frac{1}{2}\lambda \leqslant X \leqslant \frac{1}{2}\lambda$) must vanish. The pressure and wall shear forces are

$$F_p = d\,\Delta p = 12\mu u_0 \Delta P, \tag{2.12}$$

$$F_\tau = 2\mu u_0 \int_{-\frac{1}{2}\lambda}^{\frac{1}{2}\lambda} \left.\frac{\mathrm{d}U}{\mathrm{d}Z}\right|_{Z=0} \mathrm{d}X = -8\mu u_0 \lambda[(2I_1(\tfrac{1}{2}\pi) - 3I_2(\tfrac{1}{2}\pi))\,U_p + 3I_2(\tfrac{1}{2}\pi)]. \tag{2.13}$$

From the zero-drag condition ($F_\tau + F_p = 0$),

$$U_p = \frac{3I_2(\frac{1}{2}\pi) - 6I_3(\frac{1}{2}\pi)}{6I_2(\frac{1}{2}\pi) - 6I_3(\frac{1}{2}\pi) - 2I_1(\frac{1}{2}\pi)}. \tag{2.14}$$

Resulting values of U_p and ΔP are given in figure 2, which also shows numerical results obtained for the same flow by Dvinsky & Popel (1987*a*, *b*), using a finite difference form of the Stokes equations. For cylinder diameters from $\lambda = 0.6$ to $\lambda = 0.8$, close agreement is evident. For smaller diameters, lubrication theory increasingly overestimates the numerically computed particle velocity, which tends to 1.5 as the diameter approaches zero.

2.2. *The applicability of lubrication theory*

In the above example, the equations of lubrication theory were applied uniformly over the entire surface of the cylinder. The derivation of these equations is based on the assumption that the gap width is narrow compared to the lengthscale of the gap, which implies that the slope of the gap boundaries is small. This assumption is clearly not satisfied over the entire surface. Even so, lubrication theory gives good approximations to U_p and ΔP over a range of cylinder diameters. A similar conclusion was reached by Secomb *et al.* (1986) for the case of spheres in tubes.

The following argument suggests the underlying reason for this finding. We note that according to (2.4), the pressure gradient decreases in proportion to H^{-2} as H becomes large. Therefore, in the regions where the gap is relatively wide and the slope is large, the variations in pressure are much smaller than the variations in the regions of smallest gap, where the slope is small. While use of lubrication theory may lead to significant fractional errors in the estimated local pressure gradient in large-gap regions, these errors are small relative to the total fluctuations in pressure.

A further relevant property of lubrication theory was noted by Halpern & Secomb (1989). An exact similarity solution is available for Stokes flow between two rigid planes, one inclined to and sliding over the other, which it meets at one edge (Batchelor 1967). The estimates of shear stress and pressure gradient resulting from lubrication theory are within 20% of the exact values for angles between the planes as large as 45°, and much smaller for smaller angles. This indicates that errors in local pressure gradient increase relatively slowly with increasing slope.

The above arguments indicate that the equations of lubrication theory applied uniformly over the entire gap region give good approximations for pressure drop and other relevant parameters, even when the gap is not uniformly narrow. Furthermore, the examples considered above are 'worst cases' in that the region of narrowest gap is small compared to the overall gap region. If the gap is uniformly narrow over most of the surface of the particle, the relative errors involved in applying lubrication theory uniformly are likely to be much smaller than for a cylinder with the same minimum gap width. This applies to the disk-shaped particles considered here.

In the region beyond the particle, the width of the gap is the distance between the two plates. If this spacing is small compared to the other dimensions of this region (particle diameter and channel span), we may again introduce the lubrication approximations. Since the gap is uniform here, a Hele-Shaw flow results. As pointed out by Hele-Shaw (1898), these assumptions lead to discrepancies in tangential flow at solid boundaries. To accommodate the no-slip condition, boundary layers surrounding the particle and adjacent to the sides of the channel are required.

2.3. *Lubrication theory for disk-shaped particles*

The flow domain is divided into three regions (figure 3):

Region I (flat part of the disk): $0 \leqslant r \leqslant r_1$, $h = h_c \ll d$;

Region II (curved rim): $r_1 \leqslant r \leqslant r_2$, $h = h(r)$;

Region III (outside the disk): $r \geqslant r_2$, $r \sin\theta \leqslant \frac{1}{2}a$, $h = d$.

Region III includes region IIIa, the outer region, region IIIb, the boundary layer on the particle, and, for finite spans, region IIIc, the boundary layer at the edge of the channel.

We assume that the particle moves with speed $-u_p$ along the midline of the channel. Then, by symmetry, it does not rotate. Axes (r, θ, z) and (x, y, z) are fixed in the particle. Boundary conditions are $(u, v) = 0$ on the particle surface, and $(u, v) =$

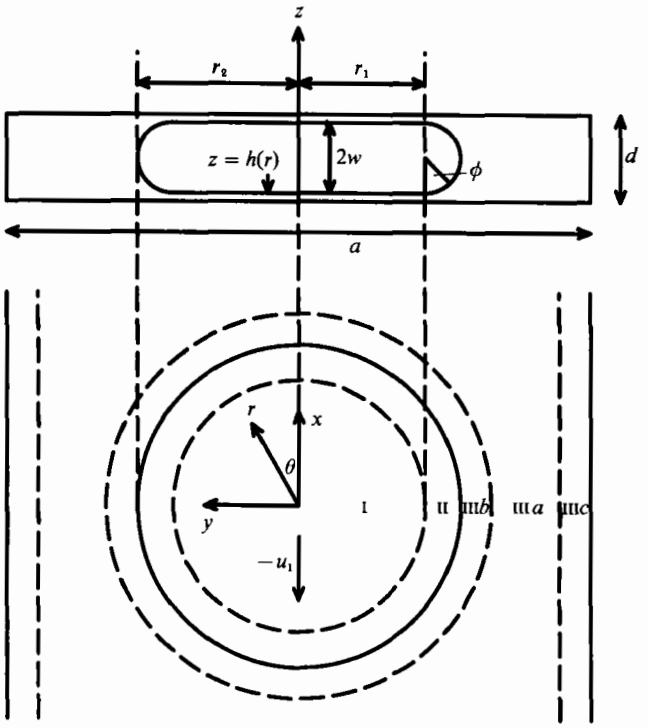

FIGURE 3. Disk-shaped particle between parallel plates, showing geometric variables and regions used in analysis.

$u_p(\cos\theta, -\sin\theta)$ at the plates, where u and v are the radial and aximuthal components of velocity. Also, $u_y = 0$ at $y = \pm\frac{1}{2}a$ where $u_y = u\sin\theta + v\cos\theta$, and $(\overline{u}, \overline{v}) \to (u_p - u_0)(\cos\theta, -\sin\theta)$ far upstream and downstream, where $\overline{u}$ and $\overline{v}$ denote z-averages, and $-u_0$ is the mean fluid velocity relative to the walls far from the particle.

The lubrication approximation to Stokes flow is used throughout the flow domain. Use of lubrication theory in region II is justified according to §2.2, even though the gap width is not uniformly small. The pressure is then $p(r, \theta)$ and the momentum equations reduce to

$$\frac{\partial p}{\partial r} = \mu\frac{\partial^2 u}{\partial z^2}, \quad \frac{1}{r}\frac{\partial p}{\partial \theta} = \mu\frac{\partial^2 v}{\partial z^2}. \tag{2.15}$$

Since the suspending fluid is incompressible, the continuity equation is

$$\frac{\partial (ru)}{\partial r} + \frac{\partial v}{\partial \theta} = 0. \tag{2.16}$$

We non-dimensionalize, setting $p(r, \theta) = p(0, 0) + 12\mu u_0 P(R, \theta)/d$, $u(r, \theta, z) = u_0 U(R, \theta, Z)$, $v(r, \theta, z) = u_0 V(R, \theta, Z)$, $u_p = u_0 U_p$, $R = r/d$, $H = h/d$, $H_c = h_c/d$, $A = a/d$, $X = x/d$, $Y = y/d$ and $Z = z/d$, and obtain

$$12\frac{\partial P}{\partial R} = \frac{\partial^2 U}{\partial Z^2}, \quad \frac{12}{R}\frac{\partial P}{\partial \theta} = \frac{\partial^2 V}{\partial Z^2}, \tag{2.17}$$

$$\frac{\partial (RU)}{\partial R} + \frac{\partial V}{\partial \theta} = 0, \tag{2.18}$$

with boundary conditions:

$$(U, V) = U_p(\cos\theta, -\sin\theta) \quad \text{at } Z = 0, \quad (U, V) = kU_p(\cos\theta, -\sin\theta) \quad \text{at} \quad Z = H,$$
$$U_Y = 0 \quad \text{at } Y = \pm\tfrac{1}{2}A, \quad (\overline{U}, \overline{V}) \to (U_p - 1)(\cos\theta, -\sin\theta) \quad \text{as } X \to \pm\infty, \quad (2.19)$$

where $k = 0$ in regions I and II and $k = 1$ in region III. Note that these equations are formulated for the gap adjacent to one wall in regions I and II, and for the entire space between the two walls in region III.

The momentum equations are integrated twice to yield the velocity components U and V:

$$U = 6\frac{\partial P}{\partial R}Z(Z-H) + U_p\cos\theta\left(1-(1-k)\frac{Z}{H}\right), \tag{2.20}$$

$$V = \frac{6}{R}\frac{\partial P}{\partial\theta}Z(Z-H) - U_p\sin\theta\left(1-(1-k)\frac{Z}{H}\right), \tag{2.21}$$

We define the following flow rates

$$Q_R = \int_0^H U\,\mathrm{d}Z = -H^3\frac{\partial P}{\partial R} + \tfrac{1}{2}(1+k)\,U_p H\cos\theta, \tag{2.22}$$

$$Q_\theta = \int_0^H V\,\mathrm{d}Z = -\frac{H^3}{R}\frac{\partial P}{\partial\theta} - \tfrac{1}{2}(1+k)\,U_p H\sin\theta. \tag{2.23}$$

Equation (2.18) implies that $\partial(RQ_R)/\partial R + \partial Q_\theta/\partial\theta = 0$, that is

$$\frac{1}{R}\frac{\partial}{\partial R}\left(RH^3\frac{\partial P}{\partial R}\right) + \frac{1}{R^2}\frac{\partial}{\partial\theta}\left(H^3\frac{\partial P}{\partial\theta}\right) = \tfrac{1}{2}(1+k)\,U_p\cos\theta\frac{\mathrm{d}H}{\mathrm{d}R}. \tag{2.24}$$

This is often referred to as Reynolds' equation (Cameron 1966).

Equation (2.24) does not have generally an exact closed-form solution for non-uniform gaps but can be solved approximately or numerically. It is solved in each region and pressure and radial flow rate are matched at the boundaries between regions, so that

$$P^{\mathrm{I}} = P^{\mathrm{II}}, \quad Q_R^{\mathrm{I}} = Q_R^{\mathrm{II}} \quad \text{at } R = R_1, \tag{2.25}$$

$$P^{\mathrm{II}} = P^{\mathrm{III}}, \quad 2Q_R^{\mathrm{II}} = Q_R^{\mathrm{III}} \quad \text{at } R = R_2, \tag{2.26}$$

where $R_1 = \mathrm{r}_1/\mathrm{d}$ and $R_2 = r_2/d$. As mentioned earlier, continuity of tangential flow rate cannot be imposed at the boundaries of region III ($R = R_2$ and $Y = \pm\frac{1}{2}A$) unless boundary layers are introduced.

3. Solutions for disk-shaped particles

3.1. *Region I: flat part of the disk*

In region I, equation (2.24) reduces to:

$$\frac{1}{R}\frac{\partial}{\partial R}\left(R\frac{\partial P}{\partial R}\right) + \frac{1}{R^2}\frac{\partial^2 P}{\partial\theta^2} = 0, \tag{3.1}$$

since the gap width is constant. The general solution with the required symmetry is:

$$P^{\mathrm{I}} = \sum_{k=0}^{\infty} C_k\left(\frac{R}{R_1}\right)^{2k+1}\cos(2k+1)\,\theta, \tag{3.2}$$

where C_k are constants. The radial flow rate is obtained using (2.22):

$$Q_R^{\mathrm{I}} = \tfrac{1}{2}U_p H_c \cos\theta - \frac{H_c^3}{R_1}\sum_{k=0}^{\infty}(2k+1)\,C_k\left(\frac{R}{R_1}\right)^{2k}\cos(2k+1)\,\theta. \tag{3.3}$$

3.2 *Region II: curved rim of the disk*

In region II, from the assumed geometry,

$$H = \tfrac{1}{2}(1-\lambda\cos\phi), \quad R = \tfrac{1}{2}\lambda\sin\phi + R_1, \tag{3.4}$$

where $\lambda = 2w/d$ and $\frac{1}{2}\pi - \phi$ is the angle between the axis of symmetry and the normal to the surface. Since the radius of the disk is large compared to the channel width, we treat the flow at each point on the rim as approximately two-dimensional and neglect θ-derivatives. Equation (2.24) becomes

$$\frac{\partial}{\partial R}\left(H^3\frac{\partial P}{\partial R}\right) = \tfrac{1}{2}U_p\cos\theta\frac{\mathrm{d}H}{\mathrm{d}R}, \tag{3.5}$$

which can be integrated to yield the pressure gradient

$$\frac{\partial P^{\mathrm{II}}}{\partial R} = \tfrac{1}{2}H^{-2}U_p\cos\theta - K(\theta)\,H^{-3} \quad \text{where } K(\theta) = Q_R^{\mathrm{II}}. \tag{3.6}$$

As in §2.1, this can be integrated from 0 to ϕ yielding

$$P^{\mathrm{II}}(\phi,\theta) = P^{\mathrm{II}}(0,\theta) + \lambda\,[U_p\cos\theta\,I_2(\phi) - 4I_3(\phi)\,K(\theta)], \tag{3.7}$$

where $I_2(\phi)$ and $I_3(\phi)$ are given by (2.9).

The neglect of θ-derivatives is based on the assumption that the radius of the particle, R_1, is much larger than the radius of the rim, $\frac{1}{2}\lambda$. For typical red blood cell dimensions, the ratio $2R_1/\lambda \approx 3.6$. Halpern (1989) solved (2.24) numerically in this case and obtained predictions of U_p within 1% of those obtained using the above approximation.

3.3 *Region IIIa: outer region*

Since $H = 1$, the pressure in the outer region satisfies Laplace's equation,

$$\frac{\partial^2 P}{\partial X^2} + \frac{\partial^2 P}{\partial Y^2} = 0, \tag{3.8}$$

in Cartesian coordinates. The boundary conditions (2.19) imply that

$$\partial P/\partial Y = 0 \quad \text{at } Y = \pm\tfrac{1}{2}A, \quad \partial P/\partial X \to 1 \quad \text{as } X \to \pm\infty. \tag{3.9}$$

This problem can be solved using potential theory (Howland 1934; Halpern 1989). We let $\Psi = X + \mathrm{i}Y$. The boundary conditions at $\Psi = \pm\frac{1}{2}\mathrm{i}A$ can be satisfied by representing the solution as a periodic function with singularities located at $(0, pA)$, where p takes all integer values. One such complex potential function is

$$\Phi_0 = \log\sin\mathrm{i}\pi\Psi/A = -\log\frac{\mathrm{i}\Psi}{A} + \sum_{p=1}^{\infty}\frac{\zeta(2p)}{p}\left(\frac{\mathrm{i}\Psi}{A}\right)^{2p}, \tag{3.10}$$

where the power series representation is convergent for $|\Psi| < A$, and ζ is the Riemann zeta function of integer argument:

$$\zeta(p) = \sum_{n=1}^{\infty}\frac{1}{n^p}. \tag{3.11}$$

Further potential functions with the desired properties are

$$\Phi_n = \frac{1}{(n-1)!}\frac{\mathrm{d}^n \Phi_0}{\mathrm{d}\Psi^n}, \tag{3.12}$$

since Φ_n also satisfies $\partial\Phi_n/\partial\Psi = 0$ on $\Psi = \pm\frac{1}{2}\mathrm{i}A$. We require only odd functions of Ψ, for which n is odd. These are:

$$\Phi_{2s+1} = \frac{(-1)^s}{\Psi^{2s+1}} + \frac{1}{A^{2s+1}}\sum_{m=0}^{\infty}\alpha_{ms}\left(\frac{\Psi}{A}\right)^{2m+1}, \tag{3.13}$$

where

$$\alpha_{ms} = (-1)^m \frac{(2(m+s)+1)!}{(2m+1)!(2s)!}\zeta(2(m+s+1)). \tag{3.14}$$

Since the pressure is even in Y and odd in X, we take the real part, $P_s = \mathrm{Re}\,(\Phi_{2s+1})$:

$$P_s = (-1)^s \frac{\cos(2s+1)\theta}{R^{2s+1}} + \frac{1}{A^{2s+1}}\sum_{m=0}^{\infty}\alpha_{ms}\left(\frac{R}{A}\right)^{2m+1}\cos(2m+1)\theta, \tag{3.15}$$

in polar coordinates. The pressure in region III can be expressed as a sum of such terms:

$$P^{\mathrm{III}} = R\cos\theta + \sum_{s=0}^{\infty} B_s P_s, \tag{3.16}$$

where B_s are unknown constants. The radial flow rate is

$$Q_R^{\mathrm{III}} = U_p\cos\theta - \frac{\partial P^{\mathrm{III}}}{\partial R} = (U_p - 1)\cos\theta - \sum_{s=0}^{\infty} B_s\frac{\partial P_s}{\partial R}. \tag{3.17}$$

For the case $A\to\infty$ (infinite span), $B_s = 0$ for $s > 0$ and $P_0 = R^{-1}\cos\theta$.

3.4 *Region IIIb: boundary layer around the particle*

The matching conditions (2.25) and (2.26) can be satisfied by solving for the coefficients C_s and B_s in regions I and III. However, the azimuthal flow rate cannot be matched at $R = R_2$, and the jump in Q_θ from region II to III is $O(1)$. The jump can be removed by inserting a boundary layer of width $O(1)$ around the edge of the particle. This boundary layer itself generates a small radial flow.

In the boundary layer, variations in the R and Z directions dominate those in the θ direction, and the Stokes momentum equation in the tangential direction reduces to

$$\frac{\partial^2 V}{\partial Z^2} + \frac{\partial^2 V}{\partial \overline{R}^2} = \frac{12}{R_2}\frac{\partial P_0^{\mathrm{III}}}{\partial\theta}, \tag{3.18}$$

where $R = R_2 + \overline{R}$ and $\partial/\partial\overline{R} \gg 1/R_2\,\partial/\partial\theta$. As usual in boundary-layer theory, the pressure is assumed not to vary across the boundary layer, and is given by P_0^{III}, the unperturbed pressure field evaluated at $R = R_2$. Let $V = V^{\mathrm{III}} + V_1$, where, from (2.21),

$$V^{\mathrm{III}} = 6Z(Z-1)\frac{1}{R_2}\frac{\partial P_0^{\mathrm{III}}}{\partial\theta} - U_p\sin\theta. \tag{3.19}$$

Hence

$$\frac{\partial^2 V_1}{\partial Z^2} + \frac{\partial^2 V_1}{\partial \overline{R}^2} = 0. \tag{3.20}$$

The boundary conditions are: $V_1 = 0$ at $Z = 0$ and $Z = 1$, and $V_1 = V_i(Z, \theta)$ at $\overline{R} = 0$, where $V_i + V^{III}$ is the tangential velocity at the interface between region II and the boundary layer. To determine V_i exactly would require the solution of the Stokes equations in region II and the boundary layer. However, V_i is constrained by several boundary conditions. At the walls ($Z = 0$ and $Z = 1$), $V_i = 0$ and, from (3.20), $\partial^2 V_i / \partial Z^2 = 0$. At the particle ($Z = \frac{1}{2}$), $V_i + V^{III} = 0$ to satisfy the no-slip condition. Also, V_i must be symmetric about $Z = \frac{1}{2}$. A polynomial approximation to V_i may be constructed by imposing these conditions. If a fourth-order polynomial is used, it is given uniquely by

$$V_i(Z, \theta) = \alpha Z(Z-1)(Z^2-Z-1), \tag{3.21}$$

where

$$\alpha = \tfrac{16}{5} U_p \sin\theta + \frac{24}{5R_2} \frac{\partial P_0^{III}}{\partial \theta}. \tag{3.22}$$

The solution to (3.20) is obtained by separation of variables:

$$V_1 = \sum_{k=0}^{\infty} \frac{96\alpha}{(2k+1)^5 \pi^5} \exp[-(2k+1)\pi\overline{R}] \sin(2k+1)\pi Z. \tag{3.23}$$

The total change to the circumferential flow in the boundary layer is

$$\Delta Q_\theta = \int_0^\infty \int_0^1 V_1 \, dZ \, d\overline{R} = 192\sigma_7 \alpha, \quad \text{where } \sigma_n = \frac{1}{\pi^n} \sum_{k=0}^{\infty} \frac{1}{(2k+1)^n}. \tag{3.24}$$

Thus, by continuity, the radial flow generated by the boundary layer is

$$\Delta Q_R = -\frac{1}{R_2} \frac{dQ_\theta}{d\theta} = -\frac{192\sigma_7}{R_2} \frac{d\alpha}{d\theta}, \tag{3.25}$$

and the matching conditions (2.26) then become

$$P^{II} = P^{III}, \quad Q_R^{III} - \Delta Q_R = 2Q_R^{II} \quad \text{at } R = R_2. \tag{3.26}$$

If a sixth-order polynomial approximation to V_i is assumed instead, one unknown parameter is introduced. If the physically reasonable restriction is imposed that V_i remains monotonic in Z on $[0, \frac{1}{2}]$, the resulting change in ΔQ_R is about 20%, at most.

The result of imposing the no-slip condition at the edge of the particle and introducing the boundary layer is to create a region in which the fluid tends to move with the particle. We might expect that the resulting external flow field is the same as for a slightly larger particle moving with the same velocity, analysed using the Hele-Shaw assumptions. Let δ be the displacement thickness, where

$$\delta = -\Delta Q_\theta / Q_\theta^{III}(R_2, \theta). \tag{3.27}$$

Then, using the continuity equation (2.18), it is easily shown that imposing the modified boundary condition (3.26) on Q_R^{III} at $R = R_2$ is equivalent to imposing the original boundary condition (2.26) at $R = R_2 + \delta$, neglecting $O(\delta^2)$ terms. When the span is infinite, δ is independent of θ, and

$$\delta = \delta_0[1 + R_2^{-2} B_0 - \tfrac{2}{3} U_p]/[1 + R_2^{-2} B_0 - U_p], \tag{3.28}$$

where $\delta_0 = 4608\sigma_7/5 \approx 0.3$, the displacement thickness when $U_p = 0$. For finite spans, δ varies around the circumference.

3.5. *Regions IIIc: boundary layers at the channel walls*

For finite span channels, boundary layers are present adjacent to the walls at $Y = \pm\frac{1}{2}A$. We assume that the flow does not vary rapidly in the X-direction near the walls. Using methods analogous to §3.4, the velocity in the X-direction is found to be

$$U = U^{\mathrm{III}} + U_1 \quad \text{where } U^{\mathrm{III}} = 6\frac{\partial P_0^{\mathrm{III}}}{\partial X} Z(Z-1) + U_p, \tag{3.29}$$

$$U_1 = \frac{48}{\pi^3}\frac{\partial P_0^{\mathrm{III}}}{\partial X}\sum_{k=0}^{\infty}\frac{1}{(2k+1)^3}\exp\left[-(2k+1)\,\pi\overline{Y}\right]\sin(2k+1)\,\pi Z, \tag{3.30}$$

and $\overline{Y} = |\frac{1}{2}A - Y|$. The flow change in the boundary layer and the transverse flow rate generated by the boundary layer are:

$$\Delta Q_X = 96\sigma_5\frac{\partial P_0^{\mathrm{III}}}{\partial X}, \quad \Delta Q_Y = -96\sigma_5\frac{\partial^2 P_0^{\mathrm{III}}}{\partial X^2}. \tag{3.31}$$

As in the previous section, the displacement thickness can be defined:

$$\delta_X = -\Delta Q_X \Big/ \int_0^1 (U^{\mathrm{III}} - U_p)\,\mathrm{d}Z = 96\sigma_5 \approx 0.32. \tag{3.32}$$

The boundary layers at the walls can be shown to have the same effect on the outer region as reducing the channel span by an amount $2\delta_X$ in the Hele-Shaw solution.

3.6. *System of equations*

To determine the Fourier coefficients C_k in region I and B_s in region III, we apply the matching conditions (2.25) and (3.26). At the boundary between regions I and II, matching the radial flow rates (3.3) and (3.6) gives:

$$K(\theta) = \sum_{k=0}^{\infty}\beta_k\cos(2k+1)\,\theta, \tag{3.33}$$

where $$\beta_0 = \tfrac{1}{2}H_c\,U_p - C_0 H_c^3/R_1, \quad \beta_k = -(2k+1)\,C_k H_c^3/R_1 \quad \text{for } k > 0, \tag{3.34}$$

By matching pressures (3.2) and (3.7) at $R = R_1$, we deduce the pressure at $R = R_2$:

$$P^{\mathrm{II}}(R_2,\theta) = \sum_{k=0}^{\infty}\gamma_k\cos(2k+1)\,\theta, \tag{3.35}$$

where $$\gamma_0 = G_0 C_0 + \lambda(I_2(\tfrac{1}{2}\pi) - 2I_3(\tfrac{1}{2}\pi)H_c)\,U_p, \quad \gamma_k = G_k C_k \quad \text{for } k > 0 \tag{3.36}$$

and $$G_k = 1 + 4(2k+1)\,\lambda I_3(\tfrac{1}{2}\pi)\,H_c^3 R_1^{-1} \quad \text{for all } k. \tag{3.37}$$

Next, we apply the matching conditions at $R = R_2$. Matching pressures implies that

$$\gamma_0 = R_2 + R_2^{-1}B_0 + \epsilon^2 R_2^{-1}\sum_{s=0}^{\infty}\alpha_{0s}B_s, \tag{3.38}$$

$$\gamma_k = \frac{(-1)^k}{R_2^{2k+1}}\left(B_k + \epsilon^{2(2k+1)}\sum_{s=0}^{\infty}\alpha_{ks}B_s\right) \quad \text{for } k > 0, \tag{3.39}$$

where $$\epsilon = \frac{R_2}{A - 2\delta_X}. \tag{3.40}$$

Matching the radial flow rates implies that

$$\beta_0 = \frac{1-3\xi_7}{2R_2^2}B_0 - \frac{\epsilon^2(1+3\xi_7)}{2R_2^2}\sum_{s=0}^{\infty}\alpha_{0s}B_s + \tfrac{1}{2}(1+2\xi_7)U_p - \tfrac{1}{2}(1+3\xi_7), \tag{3.41}$$

$$\beta_k = (-1)^k\frac{2k+1}{2R_2^{2k+2}}\left((1-3(2k+1)\xi_7)B_k - (1+3(2k+1)\xi_7)\sum_{s=0}^{\infty}\alpha_{ks}B_s\right), \tag{3.42}$$

for $k > 0$, where $\xi_7 = 1536\sigma_7/5R_2$.

To obtain the zero-drag condition, we consider the balance of forces acting on a cylindrical control volume containing the particle:

$$F_p + F_b + F_r = 0, \tag{3.43}$$

where F_r gives the shear force on the walls, F_p gives the pressure force and F_b is the force due to the shear stresses in the boundary layer surrounding the particle:

$$F_r = 2\int_0^{r_2}\int_{-\pi}^{\pi}\tau_{xz}\Big|_{z=0} r\,\mathrm{d}r\,\mathrm{d}\theta, \quad F_p = dr_2\int_{-\pi}^{\pi}p(r_2,\theta)\,\mathrm{d}\theta,$$

$$F_b = \mu u_0 dR_2\int_{-\pi}^{\pi}\int_0^1 \frac{\partial V_1}{\partial R}\Big|_{R=0}\mathrm{d}Z\sin\theta\,\mathrm{d}\theta. \tag{3.44}$$

Let $F_r = F_r^{\mathrm{I}} + F_r^{\mathrm{II}}$ where F_r^{I} and F_r^{II} are the contributions from regions I and II respectively. Then

$$F_r^{\mathrm{I}} = -2\pi\mu u_0 d\left(\frac{R_1^2}{H_c}U_p + 6H_c R_1 C_0\right), \tag{3.45}$$

$$F_r^{\mathrm{II}} = -2\pi\mu u_0 dR_2\lambda(5I_1(\tfrac{1}{2}\pi)U_p - 12I_2(\tfrac{1}{2}\pi)\beta_0), \tag{3.46}$$

where the two-dimensional approximation has been used to calculate F_r^{II} and $I_2(\frac{1}{2}\pi)$ and $I_3(\frac{1}{2}\pi)$ are given in §2.2. From (3.36), (3.44) and (3.25)

$$F_p = 12\pi\mu u_0 dR_2\gamma_0, \tag{3.47}$$

$$F_b = 2\pi\mu u_0 d\xi_5\left(3R_2^2 + 3B_0 + 3\epsilon^2\sum_{s=0}^{\infty}\alpha_{0s}B_s - 2R_2^2U_p\right), \tag{3.48}$$

where $\xi_5 = 768\sigma_s/5R_2$. The zero-drag condition (3.47) gives:

$$6H_cR_1C_0 - 12R_2\lambda I_2(\tfrac{1}{2}\pi)\beta_0 - 6R_2\gamma_0 - 3\xi_5\left(B_0 + \epsilon^2\sum_{s=0}^{\infty}\alpha_{0s}B_s\right)$$
$$+ (R_1^2/H_c + 5\lambda I_1(\tfrac{1}{2}\pi)R_2 + 2\xi_5R_2^2)U_p - 3\xi_5R_2^2 = 0. \tag{3.49}$$

Equations (3.35), (3.37)–(3.42) and (3.49) form a linear system in terms of the particle velocity, U_p, and the geometrical parameters H_c, R_1, R_2 and A, which may be solved uniquely for the unknown coefficients and the particle velocity. Corresponding equations for infinite span ($a\to\infty$) may be obtained by setting $\epsilon = 0$ in the above, while the boundary-layer effects may be excluded by omitting terms containing ξ_5 and ξ_7.

4. Results

First, results are given for infinite span ($a\to\infty$). In this case, the pressure $P(R,\theta)$ is proportional to $\cos\theta$. Figure 4 shows $P(R,0)$ for three values H_c. When the minimum gap width is small ($H_c = 0.0185$), very large pressure gradients are

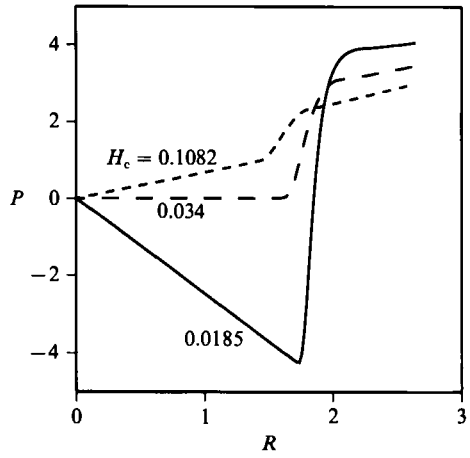

FIGURE 4. Radial variation of pressure P on the symmetry plane $\theta = 0$, for values of gap width H_c as shown.

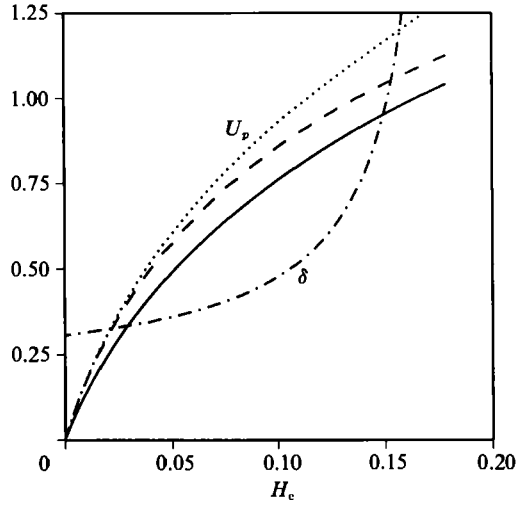

FIGURE 5. Variation of U_p and δ with H_c. ——, U_p without boundary layer; – – –, U_p with boundary layer; · · · · · ·, U_p with particle radius increased by δ_0; – · –, δ.

produced in region II, as a result of the variation of the gap width. The pressure changes in region II produce a reversal of the pressure gradient in region I. As the minimum gap width increases, the perturbation to the pressure due to the particle decreases, and the pressure gradient changes sign when $H_c \approx 0.034$.

The variation of predicted particle velocity U_p with gap width H_c is shown in figure 5, for infinite span. Particle velocity increases with increasing H_c and is equal to the mean bulk velocity when the width of the particle is about 70% of the channel width. Including the boundary layer around the particle increases U_p, by a percentage which varies from about 25% at low velocities to 10% at high velocities. Figure 5 also shows the effect of increasing R_2 by a fixed amount δ_0, independent of U_p. At low velocities, this has the same effect as inclusion of the boundary layer, as suggested in §3.4. However, this analogy breaks down at higher velocities owing to the interaction between particle velocity and the external pressure field. The variation

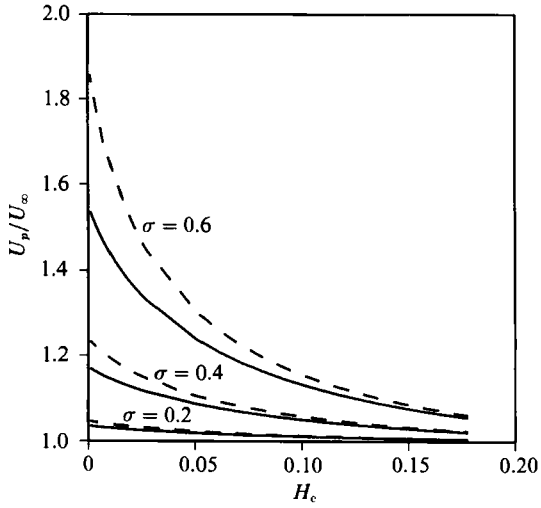

FIGURE 6. Effect of finite span ($\sigma > 0$) on particle velocity U_p. U_∞ is corresponding velocity for infinite span ($\sigma = 0$). ——, without boundary layers; ——, with boundary layers.

of displacement thickness δ with H_c is shown in figure 5. When the velocity of the particle approaches the mean bulk velocity, the denominator in (3.27) becomes small and δ increases rapidly.

Figure 6 shows the effects of finite channel span. The ratio of U_p to U_∞, the particle velocity for infinite span, is shown for three values of $\sigma = 2r_2/a$, the ratio of particle diameter to channel span, with and without boundary-layer effects. Restricting the span has the effect of increasing particle velocity. This effect is greatest for slowly moving particles, i.e. narrow gaps. As σ increases (i.e. span decreases) the velocity increase resulting from inclusion of boundary layers results is amplified. In particular, when $\sigma = 0.6$, the effective pathway available for fluid to flow around a slowly moving particle is substantially reduced by the inclusion of boundary layers on the particle and the channel edges.

Figure 7 shows pressure contours in the flow domain for two gap widths. For very narrow gaps (Figure 7*a*), the pressure variation is inverted in region I, and the pressure gradient is greatest in region II. For a larger gap width (Figure 7*b*), the particle velocity is close to the mean bulk velocity and the external field is only slightly perturbed by the particle.

5. Conclusions

The motion of a tightly-fitting red blood cell through a narrow slot may be approximated by the motion of a thin disk-shaped particle with rounded edges in the space between two parallel flat plates. Although red blood cells are deformable, the fluid mechanics of this motion may be investigated by considering rigid particles with this 'critical' shape.

Approximate solutions to the governing equations are obtained by applying lubrication theory throughout the flow domain. At the rounded edges of the particle, the formal assumptions of lubrication theory are not satisfied. However, analysis of the motion of a cylinder between two parallel plates and comparison with solutions obtained by Dvinsky & Popel (1987*b*) shows that lubrication theory yields a good approximation. In the region beyond the particle, application of lubrication theory

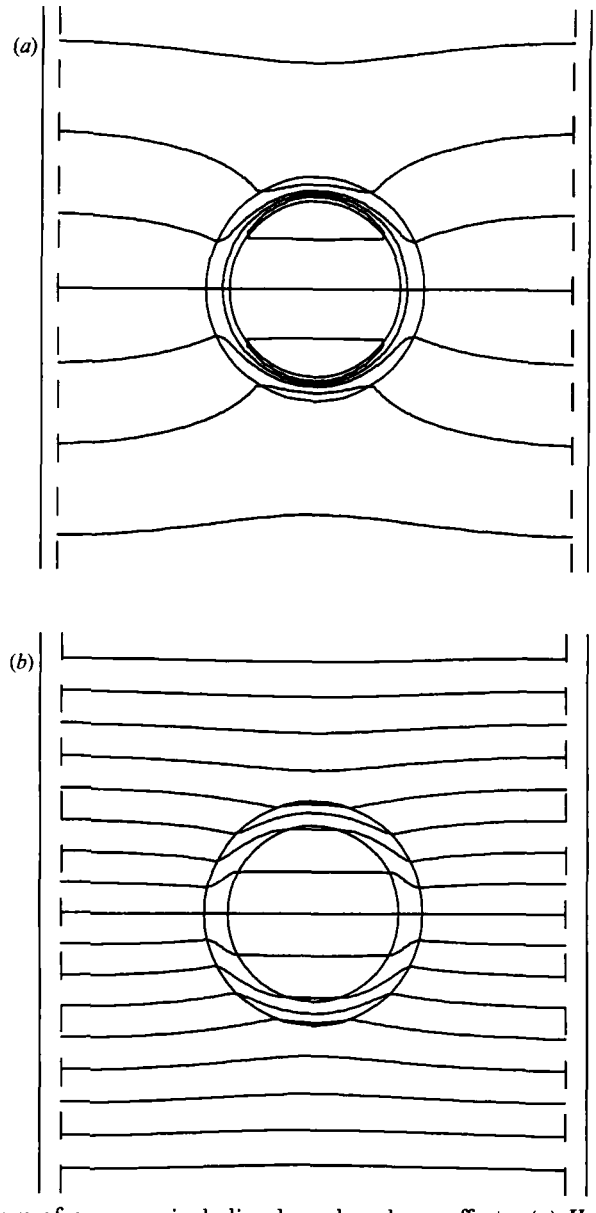

FIGURE 7. Contours of pressure, including boundary-layer effects. (*a*) $H_c = 0.0272$, $\sigma = 0.4$, $U_p = 0.44$. (*b*) $H_c = 0.14$, $\sigma = 0.4$, $U_p = 1.05$.

leads to a problem analogous to the Hele-Shaw cell, in which the no-slip condition is relaxed at the boundaries. Inclusion of boundary layers allows the no-slip condition to be satisfied. These boundary layers can significantly increase the particle velocity.

The predicted particle velocity can be smaller or larger than the mean bulk velocity, depending on the channel dimensions, and tends to zero as the gap width tends to zero. For infinite-span channels, particle velocity approaches mean bulk velocity when the particle width is about 70% of the channel width. Decreasing the channel span decreases the space available for fluid to flow around the particle, leading to increased particle velocity.

In cylindrical tubes, axisymmetric particles always travel faster than the mean bulk flow (Halpern & Secomb 1989). If the particle is tightly fitting, the driving pressure in the tube is concentrated across the particle, and the mean bulk velocity is reduced. In a channel, the situation is different in that fluid can bypass the particle, and the pressure drop is not concentrated in the immediate vicinity of the particle. For infinite-span channels, the maximum pressure gradient experienced by the particle is twice the pressure gradient in the absence of the particle.

The tendency of red blood cells to travel faster than the mean flow in cylindrical tubes leads to the Fahraeus effect: the volume fraction of red blood cells (haematocrit) within the tube is less than their fractional contribution to the flow entering and leaving the tube (Secomb *et al.* 1986). Conversely, when the red cell velocity in a slot is lower than the mean velocity, the haematocrit in the slot is increased. This probably contributes to the observation that the haematocrit in the spleen is higher than in other parts of the body (Gibson *et al.* 1946).

This work was supported by National Institutes of Health grants HL34555, HL17421 and HL07249. The above work has been performed in partial fulfilment of the requirement for the Ph.D. degree of D.H. at the University of Arizona.

REFERENCES

Batchelor, G. K. 1967 *An Introduction to Fluid Dynamics*. Cambridge University Press.

Cameron, A. 1966 *The Principles of Lubrication Theory*. Longmans Green.

Dvinsky, A. S. & Popel, A. S. 1987*a* Motion of a rigid cylinder between parallel plates in Stokes flow. Part 1: Motion in a quiescent fluid and sedimentation. *Comput. Fluids* **15**, 385–404.

Dvinsky, A. S. & Popel, A. S. 1987*b* Motion of a rigid cylinder between parallel plates in Stokes flow. Part 2: Poiseuille and Couette flow. *Comput. Fluids* **15**, 405–419.

Gibson, J. G., Seligman, A. M., Peacock, W. C., Aub, J. C., Fine, J. & Evans, R. D. 1946 The distribution of red cells and plasma in large and minute vessels of the normal dog, determined by radioactive isotopes of iron and iodine. *J. Clin. Invest.* **25**, 848–857.

Halpern, D. 1989 The squeezing of red blood cells through tubes and channels of near-critical dimensions. PhD dissertation, University of Arizona, Tucson.

Halpern, D. & Secomb, T. W. 1989 The squeezing of red blood cells through capillaries with near-minimal diameters. *J. Fluid Mech.* **203**, 381–400.

Hele-Shaw, H. J. S. 1898 The flow of water. *Nature* **58**, 34–36.

Howland, R. C. J. 1934 Potential functions with periodicity in one coordinate. *Proc. Camb. Phil. Soc.* **30**, 315–326.

Özkaya, N. 1986 Viscous flow of particles in tubes: Lubrication theory and finite element models. PhD dissertation, Columbia University, New York.

Özkaya, N. & Shalak, R. 1983 The steady flow of particles in a tube. In *1983 Advances in Bioengineering* (ed. D. L. Bartel), pp. 9–10. ASME, New York.

Secomb, T. W., Skalak, R., Özkaya, N. & Gross, J. F. 1986 Flow of axisymmetric red blood cells in narrow capillaries. *J. Fluid Mech.* **163**, 405–423.

Sommerfeld, A. 1904 Zur hydrodynamischen theorie der schmiermittelreibung. *Z. Math. Phys.* **40**, 97–155.